Available online at www.sciencedirect.com
SCIENCE DIRECT
Precambrian Research 146 (2006) 120–137
Precambrian Research
www.elsevier.com/locate/precamres

Geochronological constraints on tourmaline formation in the Western Fold Belt of the Mount Isa Inlier, Australia: Evidence for large-scale metamorphism at 1.57 Ga?

R.J. Duncan [a,*], A.R. Wilde [a], K. Bassano [b], R. Maas [b]

[a] *pmd*CRC, School of Geosciences, Monash University, Clayton, Vic. 3800, Australia*
[b] *pmd*CRC, School of Earth Sciences, Melbourne University, Parkville, Vic. 3010, Australia*

Received 24 May 2005; received in revised form 8 January 2006; accepted 19 January 2006

Abstract

Boron metasomatism during two deformational events resulted in tourmaline formation in parts of late Palaeoproterozoic Eastern Creek Volcanics of the Western Fold Belt of the Mount Isa Inlier. Despite low U/Pb ratios (≪1, as measured by laser ablation ICP-MS). When the step leaching process was applied to the tourmaline it process extracted Pb fractions with $^{206}Pb/^{204}Pb$ up to 76, illustrating the method's ability to efficiently separate radiogenic and common Pb that are hosted in different crystal lattice sites. Tourmaline from two syn-D_2 metamorphic/hydrothermal veins at Anderson's Lode and Eldorado yield similar Pb step-leaching ages of 1573 ± 12 and 1577 ± 48 Ma, respectively. Tourmaline from a post-D_2, but, pre-D_{3a}, vein at King was dated at 1528 ± 51 Ma. Although there is evidence to suggest some contribution from U-rich inclusions (i.e., zircon and monazite) to some leach steps, the isochrons are thought to provide robust ages for hydrothermal tourmaline formation during two discrete thermal events. This is supported by estimates of Pb closure temperatures in tourmaline derived from ionic porosity models. The ~1575 Ma ages for D_2 also reflect the main metamorphic event in the Western Fold Belt, but are ~40 myr older than accepted age estimates for this episode. The revised timing for peak metamorphism/tectonism in the Western Fold Belt corresponds with the age of metamorphism in the Eastern Fold Belt, suggesting broadly coeval tectonic histories across the entire Inlier from at least 1600 Ma.

Keywords: Pb–Pb stepwise leaching (PbSL); Tourmaline; Metamorphism; Isan Orogeny; Western Fold Belt; Mount Isa Inlier

1. Introduction

Between ~1590 and 1500 Ma an extended period of crustal shortening termed the Isan Orogeny, occurred within the Mount Isa Inlier of Northern Australia (e.g., O'Dea et al., 1997). In this paper we present structural and geochemical evidence for the crystallization of tourmaline in the Western Fold Belt of the Mount Isa Inlier (Fig. 1) near the peak of regional metamorphism during the Isan Orogeny. Many details of this protracted orogeny, in particular the timing of the main D_2 deformational/metamorphic phase, remain controversial. To further refine the geochronological relationships between deformation, metamorphism and metasomatism, Pb–Pb stepwise leaching (PbSL) was used to date several occurrences of well-defined pre- to syn-D_2 and post-D_2/pre-D_{3a} metamorphic/hydrothermal tourmaline from veins in the Palaeoproterozoic Eastern Creek Volcanics (ECV) metabasalts and metasedimentary rocks of the Myally Sub-group (Duncan and Wilde, 2004). Although there is very little published data on tourmaline PbSL (Frei and

* Corresponding author. Tel.: +61 3 9905 1127; fax: +61 3 9905 4903.
E-mail address: robert.duncan@sci.monash.edu.au (R.J. Duncan).

0301-9268/$ – see front matter © 2006 Elsevier B.V. All rights reserved.
doi:10.1016/j.precamres.2006.01.010

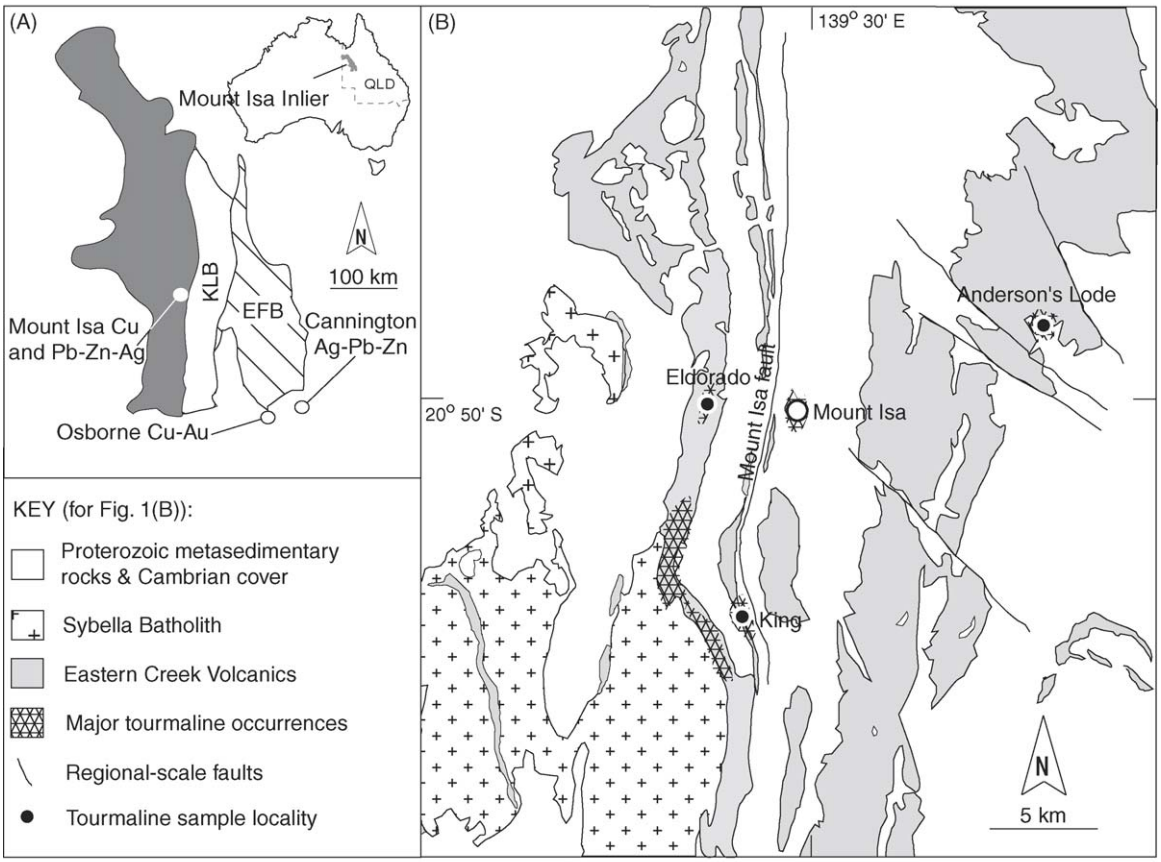

Fig. 1. (A) Location of Mount Isa Inlier and its tectono-stratigraphic divisions; WFB (Western Fold Belt), KLB (Kalkadoon-Leichhardt Belt) and EFB (Eastern Fold Belt). (B) Simplified geologic map of the Western Fold Belt around Mount Isa, showing location of mineral deposits, distribution of tourmaline alteration and location of tourmaline samples dated in this study.

Pettke, 1996), the method appears to be the only viable option available, given the low U/Pb of the tourmalines (see below). If D_2 can be constrained both directly, and indirectly by a younger age for the pre-D_{3a} sample, it would go a long way towards resolving the current debate over the duration of compressional tectonism in the region and the metamorphic history in the inlier as a whole (e.g., MacCready et al., 1998; Perkins and Wyborn, 1998; Giles and Nutman, 2002).

2. Geologic framework

The Mount Isa Inlier is a poly-deformed mobile fold belt that underwent a protracted tectonic history and hosts the world-class Cu ore bodies at Mount Isa. The terrane is divided into three tectono-stratigraphic domains (that trend north to south), known as the Western Fold Belt (WFB), Kalkadoon-Leichhardt Belt (KLB) and the Eastern Fold Belt (EFB), this study focuses on the cover sequences of the WFB (Fig. 1).

Most of the WFB originated as supracrustal volcanic and sedimentary rocks that were (1) deposited in a series of intracontinental extension-related basins between 1785 and 1650 Ma (Eriksson et al., 1994); (2) intruded in parts by the Sybella Batholith around 1670–1650 Ma (Page and Bell, 1986; Connors and Page, 1995); (3) multiply deformed and regionally metamorphosed during the Isan Orogeny from 1590 to 1500 Ma (Fig. 2; Connors and Lister, 1995; O'Dea et al., 1997; Betts et al., 1998) and (4) exhumed from 750 Ma onwards (Spikings et al., 2002).

The effects of the Isan deformation are widely debated and attempts to correlate the work of previous authors are problematic. The structural nomenclature adopted here is after Connors et al. (1992) and Connors and Lister (1995) and is specific to the WFB. The most widespread structural elements are syn- to post-peak metamorphic in timing (D_2) and are the result of east–west directed compression. D_2 produced asymmetric, north to west-north-west plunging folds, with a south-west to west

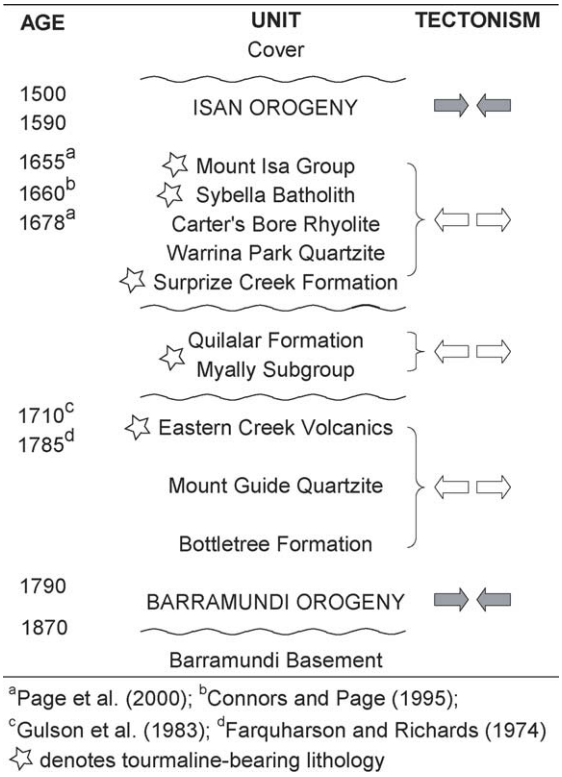

Fig. 2. Generalized tectono-stratigraphic evolution of the Western Fold Belt from 1870 to 1500 Ma, highlighting major tourmaline-bearing units. Compressional tectonism is indicated by shaded convergent arrows and extensional tectonism is indicated by white divergent arrows.

moderately dipping cleavage with an associated stretching lineation. D_{3a} was dominated by north–south striking shear-zone development and D_{3b} involved west over east thrusting and associated crenulation cleavage development. Peak metamorphism was interpreted to have taken place between D_2 and D_{3a} (Connors and Lister, 1995).

3. Previous geochronology of the Isan Orogeny

Despite many attempts, the absolute timing of the Isan Orogeny remains controversial. Fig. 3 provides a summary of existing published geochronological data. Rb–Sr whole rock dating ages for deformation in the Sybella Batholith indicate three discrete events: D_1 at 1610 ± 13 Ma, D_2 at 1544 ± 12 Ma and D_3 at 1510 ± 13 Ma (Page and Bell, 1986; Bell, 1983).

Other geochronological studies have focussed on the timing of HT/LP regional peak-metamorphic event which overprints contact metamorphism around the 1670 Ma Sybella Batholith in the WFB (Rubenach, 1992). The oldest age for peak metamorphism of 1575 Ma (no error reported) is derived from a U–Pb CHIME (chemical isochron method) analysis of monazite from the ECV approximately 4 km west of the Mount Isa Fault (Fig. 1; Hand and Rubatto, 2002). Syntectonic tourmaline-bearing pegmatites, located 25 km south of Mount Isa, have yielded $^{207}Pb/^{206}Pb$ SHRIMP zircon ages of 1532 ± 7, 1565 ± 5 and 1480 ± 14 Ma (Connors and Page, 1995), precluding any genetic link between the pegmatites and the Sybella Batholith. Connors and Page (1995) favoured the 1532 Ma age as representing the emplacement of the pegmatites, and thus the age of peak metamorphism and crustal anatexis. Additional constraints on peak metamorphism in the WFB are provided by $^{40}Ar/^{39}Ar$ biotite ages of 1554 ± 2 and 1534 ± 4 Ma from the Anderson's Lode U deposit, 15 km east of Mount Isa; these ages reflect post-peak-metamorphic cooling (Perkins et al., 1999).

The available geochronological data suggest that the metamorphic peak in the EFB could be as much as 50 myr older than in the WFB (e.g., Perkins and Wyborn, 1998). This is supported by 1584 ± 17 Ma SHRIMP U–Pb ages for metamorphic zircon overgrowths in paragneiss from the EFB (Page and Sun, 1998). Similar ages (1577 ± 5 and 1578 ± 4 Ma) were obtained from SHRIMP U–Pb monazite analyses of upper amphibolite paragneiss and pegmatites at the Cannington Pb–Ag–Zn deposit (Giles and Nutman, 2002). Perkins and Wyborn (1998) reported $^{40}Ar/^{39}Ar$ ages of ca. 1590 and 1568 ± 4 Ma on actinolite and biotite, respectively, from the Osborne Cu–Au deposit in the EFB. All these ages appear to place amphibolite facies metamorphism in the EFB at between 1580 and 1570 Ma (Fig. 3B), in contrast to the preferred ~1530 Ma age for peak metamorphism in the WFB (e.g., Connors and Page, 1995). This apparent diachroneity has led to the development of bipartite tectonic evolutionary models for the inlier, during which an early phase (ca. 1600–1550 Ma) of westward thin-skinned thrusting is restricted to the EFB and a later (ca. 1550–1500 Ma) east–west shortening typifies the WFB (MacCready et al., 1998; Giles and Nutman, 2002).

Plutons of the Williams and Naraku Batholiths form a large part of the EFB (e.g., Wyborn et al., 1998). The majority of the intrusions are not deformed or metamorphosed and were emplaced during the protracted Williams thermal event either in the interval 1545–1520 Ma or closer to 1500 Ma (e.g., Page and Sun, 1998; Oliver et al., 2004). The earlier group of plutons are temporally equivalent to the accepted ~1530 Ma age of Connors and Page (1995) for peak metamorphism in the WFB (Fig. 3).

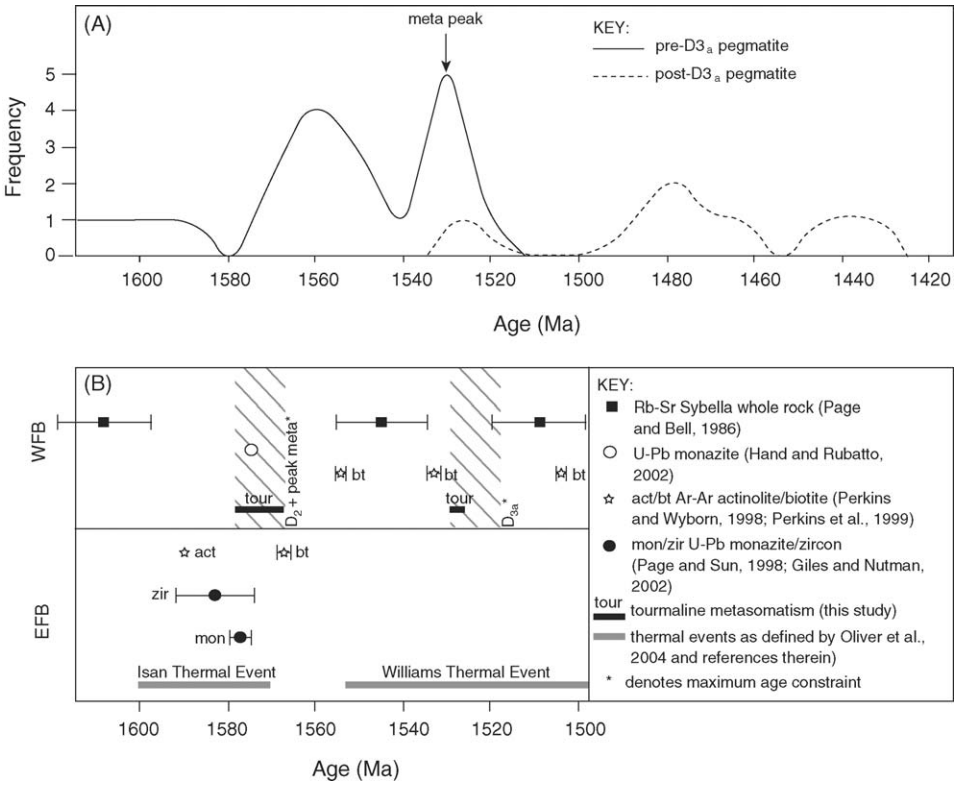

Fig. 3. Summary of previous results from geochronological studies aimed at dating deformation events and metamorphism during the Isan Orogeny in both the WFB and EFB. (A) Frequency distribution of Pb–Pb SHRIMP age data from Connors and Page (1995) used to constrain peak metamorphism in the Western Fold Belt. (B) Comparison of ages from the WFB and EFB from various sources. Note that both plots have the same *x*-axis age scale.

4. Pb stepwise leaching technique

In order to date high-grade portions of metamorphic P-T-t loops a radiogenic isotope system with a high closure temperature is required. U–Pb analyses of metamorphic monazite and zircon generally provide a precise age, but our understanding of their relationship with metamorphic reactions and micro-structures as defined by major rock forming minerals is still rudimentary (e.g., Roberts and Finger, 1997; Williams and Jercinovic, 2002; Müller, 2003). An alternative approach involves dating metamorphic minerals directly (e.g., Mezger et al., 1991; Lanzirotti and Hanson, 1997). The U–Pb thermochronometric system features prominently in such studies because several of the common metamorphic phases have reasonably high initial U/Pb ratios, producing accurate ages. However, bulk U/Pb analyses of metamorphic minerals may be severely biased if the U–Pb budgets are influenced by the presence of micro-inclusions in the host, such as zircon or monazite (Frei, 1996; Frei et al., 1997; Vance et al., 1998).

An elegant alternative to bulk methods was introduced by Frei and Kamber (1995). They demonstrated that sequential acid leaching could be used to generate well-defined Pb–Pb isochrons from relatively old (>400 Ma) minerals with low U contents, that would be unsuitable for conventional bulk U–Pb dating. The simple PbSL technique requires no spike or common Pb corrections and can produce ages with adequate precision (<1% in favourable cases) from a large range of minerals, preferably older than ca. 1 Ga. A major advantage of PbSL is the ability to use the $^{208}Pb/^{206}Pb$ ratio, or the time-integrated Th/U ratio inferred from it, to identify leach steps that contain anomalous Pb that may be inherited from zircon (low Th/U) or monazite (high Th/U) impurities. Therefore, it is crucial to characterize samples in terms of geochemical composition (especially Th/U ratios) and identify any included phases. In the present study this was achieved by using results from electron microprobe and laser ablation ICP-MS analyses and scanning electron microscopic imaging.

PbSL has been used to date a range of silicate minerals (titanite, hornblende, clinopyroxene, orthopyroxene, epidote, garnet and staurolite; Frei et al., 1995; Frei and Kamber, 1995; Dahl and Frei, 1998; Kamber et al., 1998; Dahl et al., 1999; Buick et al., 1999), as well as sulphides

and magnetite (Frei and Pettke, 1996; Frei et al., 1998; Collerson et al., 2002). Frei and Pettke (1996) were the first to apply PbSL dating to hydrothermal tourmaline from the shear-zone hosted Kimberley Au deposit in the Zimbabwe Craton. Their results demonstrate that PbSL on tourmaline could produce precise isochron ages that were in agreement with other geochronological data, and that the tourmaline Pb isotope systematics were not affected by later hydrothermal events or intense subsequent shear-zone development. This work provided the main foundation for the present study.

5. Sample descriptions

Tourmaline-rich lithologies are abundant in specific areas around Mount Isa (Fig. 1). Tourmaline is especially prevalent in the ECV (both in basalts and interflow sediments) west of the Mount Isa Fault (Fig. 2). In this area tourmaline occurs in quartz-K feldspar-mica-apatite pegmatites around the contact of the Sybella Batholith, and also as apparently stratabound, but not stratiform, tourmalinites (quartz veins with >15 vol.% tourmaline; Slack (1982)). These tourmalinites are representative of extensive regional silicification. Less widespread tourmaline occurrences have been identified in the ECV to the east of Mount Isa. It is also present as an accessory phase in the silica-dolomite alteration around the Mount Isa Cu ore bodies (Mathias and Clark, 1975). No studies have previously documented the regional extent of the tourmaline-rich lithologies. The three samples selected for dating were from within 25 km radius of Mount Isa and are in close proximity to small mineral occurrences (Fig. 1).

Sample RD03066 from Anderson's Lode (a small U deposit hosted by the ECV; Gregory et al., 2005) is a quartz-fibrous tourmaline vein deformed by D_{3a} shearing (sinistral kinematic indicators are seen at outcrop and thin section scales; Fig. 4A). The sub- to euhedral tourmaline crystals (30% of the vein) are glomerocrystic, vary from <0.1 to 8 mm in length and are aligned sub-parallel with S_2 (Fig. 4B), moderately pleochroic and do not exhibit optical zoning. The vein quartz exhibits extensive annealing textures. Host rock tourmaline is overprinted by a biotite-chlorite peak-metamorphic matrix (Fig. 4C). These relationships suggest that tourmaline crystallization was pre- to early syn-metamorphic and syn-D_2 to pre-D_{3a} in timing. Paragenetically associated with the quartz-tourmaline vein are minor amounts of titanite, chlorite, pyrite and chalcopyrite.

Sample AW02028 is from a coarse-grained quartz-tourmaline-K-feldspar-mica pegmatite (Fig. 5A) adjacent to the Eldorado U deposit, which is hosted by amphibolitic ECV (Gregory et al., 2005). The anhedral tourmaline crystals are upto 4 mm in diameter and contain quartz and K-feldspar inclusions (Fig. 5B). The

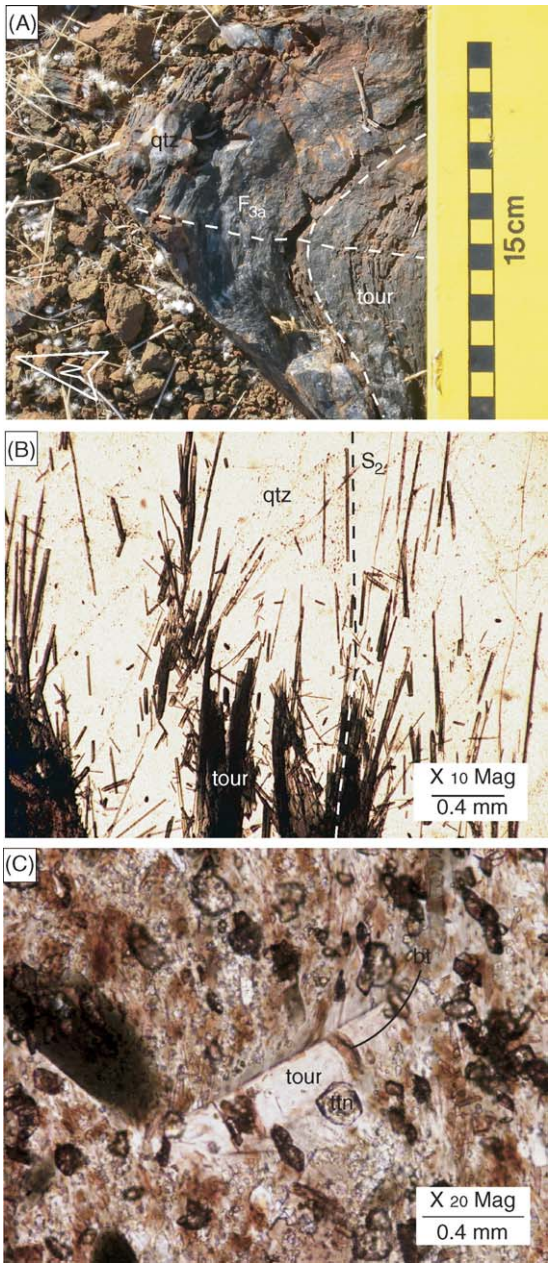

Fig. 4. (A) Field photograph of quartz-tourmaline vein from Anderson's Lode (sample RD03066; AMG 355270 mE 7714556 mN). (B) Photomicrograph (PPL) of sample RD03066 from Anderson's Lode with acicular tourmaline crystals (tour) aligned sub-parallel to the S_2 fabric hosted by quartz (qtz). (C) Photomicrograph (PPL) of a sample from the host rock of the quartz-tourmaline vein at Anderson's Lode that demonstrates euhedral tourmaline (tour) overprinted by biotite (bt) and titanite (ttn).

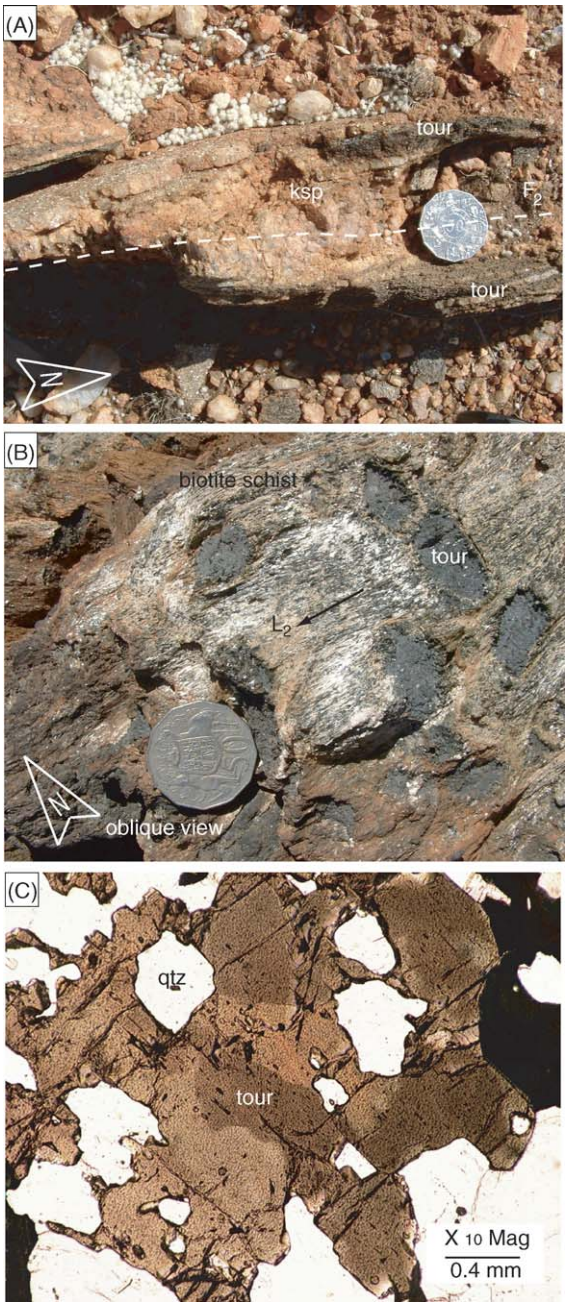

Fig. 5. (A) Field photograph of K-feldspar (ksp)-quartz (qtz) pegmatite with tourmaline (tour) selvedge (sample AW02028; AMG 337406 mE 7710378 mN) at Eldorado that is boudinaged by S_2. (B) Field photograph of tourmaline pegmatite selvedge (hosted by biotite schist) at Eldorado (adjacent to sample AW02028), tourmaline pseudomorphs subhedral cordierite poikiloblasts and it also forms a steeply plunging mineral lineation (L_2). (C) Photomicrograph (PPL) of a sample AW02028 that shows graphic intergrowth of tourmaline and quartz.

tourmaline displays strong pleochroism and some fine optical zoning. The pegmatite is parallel to the S_2 fabric and is boudinaged by D_3 structures. Tourmaline in the pegmatite selvedges defines a steeply plunging mineral lineation (L_2) and pseudomorphs cordierite poikiloblasts in the wall rock (Fig. 5C). Accessory pegmatite mineral phases include magnetite, ilmenite and rutile. Primary two phase liquid–vapour fluid inclusions within tourmaline from this sample contain upto 436 ppm U (Duncan and Wilde, 2004).

Sample RD03024 is from the King Cu deposit, 25 km south of Mount Isa (Connors, 1992). Tourmaline in this location is stratabound, but not stratiform within quartzite and psammopelitic units of the Myally subgroup. Tourmaline appears to be rhythmically layered with quartz on a decimetre scale. Tourmaline growth overprints the S_2 fabric, defined by biotite and sillimanite, and is deformed by a D_3 NNW-trending shear zone and NNW gently plunging meso-scale folds (Fig. 6A). The sample consists of coarse-grained (up to 2 cm) euhedral zoned glomerocrysts of tourmaline and coarse-grained strained quartz, along with minor amounts of titanite, sphalerite, ilmenite and rutile (Fig. 6B).

6. Analytical techniques

6.1. Electron microprobe analyses (EMP)

Table 1 summarizes quantative microprobe analyses that were performed using a Cameca Electron Microprobe SX 50 at the University of Melbourne. Operating conditions were a 25 nA beam, an acceleration potential of 14.93 kV and a 20 s count time using natural mineral standards. To characterize compositional zoning patterns micrometric core to rim steps were implemented. Tourmaline analyses were normalized on the basis of 19 cations, three B cations, four hydroxyl groups per unit formula and insignificant Li content (Henry and Dutrow, 1996; Hawthorne and Henry, 1999). All Fe was assumed to be in the ferrous state.

6.2. Laser ablation ICP-MS

In-situ trace element analyses (U, Th and Pb) were acquired using the laser ablation ICP-MS facility at Monash University. This facility consists of a Finnigan Element Sector ICP-MS coupled to a Merchantek LUV 266 nm Nd-YAG laser. For this study, the laser was operated with a 10 Hz laser frequency, laser energy of 1.04–1.13 mJ, a spot diameter of 50 μm and a 60 s data acquisition period. Data were quantified against NIST standard glasses and by internal normalization to

Table 1
Tourmaline electron microprobe data with calculated structural chemical formulae

	RD03024		AW02028		RD03067	
	Core ($n=4$)	Rim ($n=5$)	Core ($n=3$)	Rim ($n=2$)	Core ($n=4$)	Rim ($n=3$)
SiO_2	34.799	34.418	35.432	35.351	36.096	35.459
Al_2O_3	30.750	30.383	30.715	30.512	29.905	28.953
TiO_2	0.600	0.702	0.685	0.680	0.164	0.876
FeO	8.814	9.098	10.026	10.123	11.263	11.654
MnO	0.025	0.057	0.328	0.311	0.067	0.037
MgO	6.483	6.569	5.999	6.110	6.133	6.285
Cr_2O_3	0.021	0.013	0.039	0.018	0.002	0.002
CaO	0.719	0.826	0.577	0.689	0.598	1.033
Na_2O	2.115	2.143	2.338	2.276	2.324	2.185
K_2O	0.021	0.039	0.051	0.041	0.022	0.028
Total	84.346	84.247	86.189	86.111	86.574	86.514
Calculated structural formulae based on 29 oxygen anions and 3 stoichiometric boron cations per unit formula[a]						
B	3.000	3.000	3.000	3.000	3.000	3.000
Si	5.957	5.902	5.967	5.961	6.063	5.987
Al T-site	0.043	0.098	0.033	0.039	0.000	0.000
Al Z-site	6.000	6.000	6.000	6.000	5.920	5.761
Al Y-site	0.161	0.043	0.064	0.026	0.000	0.000
Al_{tot}	6.204	6.141	6.097	6.064	5.920	5.761
Cr	0.003	0.002	0.005	0.002	0.000	0.000
Ti	0.077	0.091	0.087	0.086	0.021	0.111
Fe	1.262	1.305	1.412	1.428	1.582	1.645
Mn	0.004	0.008	0.047	0.044	0.010	0.005
Mg	1.655	1.679	1.506	1.536	1.536	1.582
Z- and Y-site$_{tot}$	2.997	3.083	3.052	3.094	3.148	3.344
Ca	0.132	0.152	0.104	0.124	0.108	0.187
Na	0.702	0.713	0.763	0.744	0.757	0.715
K	0.005	0.008	0.011	0.009	0.005	0.006
X-site □	0.162	0.127	0.121	0.123	0.131	0.092
X-site$_{tot}$	0.838	0.873	0.879	0.877	0.869	0.908
Na/(Na + K)	0.994	0.988	0.986	0.988	0.994	0.992
Na/(Na + Ca)	0.842	0.824	0.880	0.857	0.876	0.793
X-site □/(Na + X-site □)	0.187	0.152	0.137	0.141	0.147	0.114
OH	4.000	4.000	4.000	4.000	4.000	4.000
Fe/(Fe + Mg)	0.433	0.437	0.484	0.482	0.507	0.510
Mineral name	Dravite	Dravite	Dravite	Dravite	Schorl	Schorl

Core and Rim denote relative grain position, n = number of analyses.
[a] According to method in Henry and Dutrow (1996) and Hawthorne and Henry (1999).

Table 2
In-situ laser ablation ICP-MS data for U, Th and Pb contents of core and rim portions of tourmaline grains and NIST 612 standard glasses

	RD03066		AW02028		RD03024		NIST 612 unknown[a]		NIST 612 glass[b]	
	Core ($n=4$)	Rim ($n=4$)	Core ($n=4$)	Rim ($n=4$)	Core ($n=4$)	Rim ($n=3$)	Mean ($n=16$)	1σ	Mean	1σ
Pb (ppm)	13.98	14.84	8.15	7.14	4.56	5.55	38.58	1.25	38.96	1.84
Th (ppm)	0.03	0.02	3.56	1.50	0.24	0.29	37.51	1.05	37.15	1.23
U (ppm)	0.04	0.02	2.18	0.77	0.07	0.09	36.90	0.83	37.23	0.72
Th/U	0.81	1.39	1.63	1.96	3.56	3.22				

Core and Rim denote relative grain position, n = number of analysis.
[a] This study.
[b] Preferred values reported in Pearce et al. (1997).

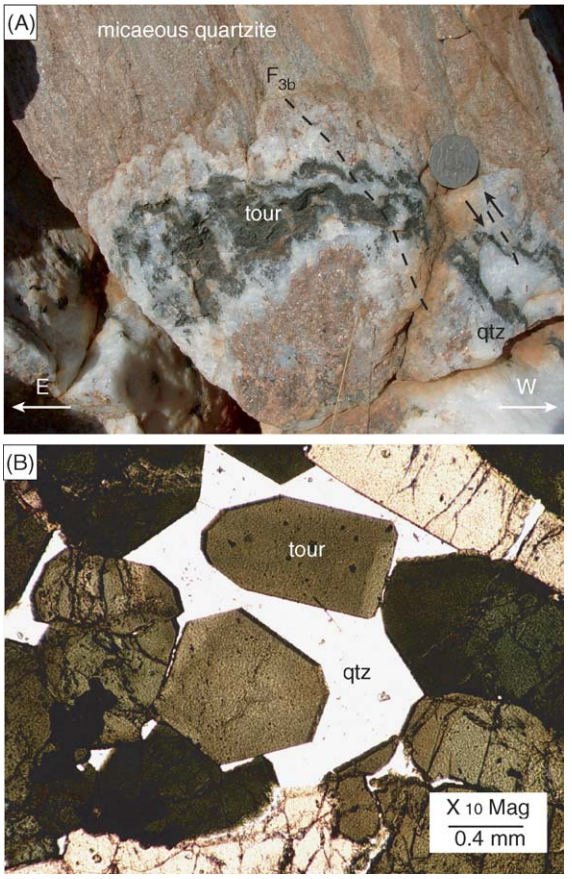

Fig. 6. (A) Field photograph of quartz (qtz)-tourmaline (tour) vein (sample RD03024; AMG 338417 mE 7685015 mN) hosted by micaceous quartzite close to King; it exhibits overturned, asymmetrical meso-scale folding and small-scale reverse faulting characteristics of D_{3b} (sense of movement is west over east). (B) Photomicrograph (PPL) of a sample RD03024 that shows euhedral nature of tourmaline grains with some evidence of compositional zoning.

Na; data quality was assessed by analysing NIST 612 standard glass during the analytical period (Pearce et al., 1997). All data processing was undertaken using the GLITTER (v.4) software of van Achterbergh et al. (2001). The data are given in Table 2.

6.3. Scanning electron microscopy

Back-scattered electron (BSE) images of the tourmaline samples were obtained at the University of Melbourne, using a Philips XL-30 Environmental Scanning Electron Microscope (ESEM), combined with a X-ray Energy Dispersive Detector (Oxford INCA-300).

6.4. Pb stepwise leaching

PbSL studies were carried out at the University of Melbourne, using tourmaline carefully handpicked from 200 to 400 μm heavy mineral fractions. Following repeated cleaning in hot distilled water, the tourmalines were sequentially leached with a HCl–HBr mix, HBr, HNO_3 and HF on a hot plate at ∼100 °C (Table 3). A total of 5–7 separate leachates, including total residue dissolution in HF, were obtained for each sample. Pb was extracted on 0.1 ml (12 mm × 4 mm) columns of EiChrom™ Sr resin (50–100 μm), according to the method of Thériault and Davies (1999). A 2–3 mm bed of prefilter resin was placed underneath the Sr resin bed to reduce co-elution of organic material and Pb in 6 M HCl. The EiChrom™ Sr resin technique provides Pb fractions of adequate purity from difficult matrices in a single pass with reasonable yields and acceptable blanks (e.g., Gale, 1996; Thériault and Davies, 1999).

All acids used were distilled in quartz or Teflon; HBr was prepared by bubbling HBr gas into distilled water. Acid blanks were <1 pg/g Pb (<3 pg/g Pb for HF) and distilled water was produced in an ELGA water purification system had <0.5 pg/g Pb. Total procedural blanks for this study were in the range of 20–40 pg Pb.

Pb isotopic ratios were measured by multi-collector ICP-MS, using a Nu Plasma MC-ICP-MS equipped with a CETAC-Adrius desolvating nebulizer and Glass Expansion Opalmist nebulizer, providing a sensitivity of around 100 V/ppm Pb at 30 μl/min uptake (Woodhead, 2002). Pb, Tl and ^{202}Hg, were measured on Faraday collectors in static mode. Mass bias was corrected for using a Tl-doping technique which produces data with external precisions ($2\sigma_m$) near ±0.03% (Woodhead, 2002).

7. Results

7.1. Tourmaline composition

EMP analyses (Table 1) demonstrate that all the tourmaline samples lie compositionally on the schorl (end member $NaFe_3Al_6(BO_3)_3(OH)_3OH$) to dravite (end member $NaMg_3Al_6(BO_3)_3(OH)_3(OH)$) solid solution. Na/(Na + Ca) and Fe/(Fe + Mg) ratios have been used to assign mineral names (Fig. 7).

Tourmaline from Anderson's Lode is schorlitic in composition (Fe/(Fe + Mg) = 0.51), whereas tourmalines from Eldorado and King are dravitic, with Fe/(Fe + Mg) ratios of 0.43 and 0.48, respectively. The latter displays oscillatory zoning in some grains, however, this is not reflected in significant core to rim chemical variations. Compositions of this type are considered to be metamorphic in origin (e.g., Henry and Guidotti, 1985) and the Fe/(Fe + Mg) values fall in the range reported for tourmaline in other Australian Proterozoic terranes, such as the Broken Hill (0.31–0.66; Slack

Table 3
Pb isotope data derived from stepwise leaching of tourmaline

Sample	Acid	Time	Code	Pb (ng)	$^{206}Pb/^{204}Pb$	2S.E. (%)	$^{207}Pb/^{204}Pb$	2S.E. (%)	$^{208}Pb/^{204}Pb$	2S.E. (%)
RD03066	1.5N HBr–2N HCl[a]	5 min	[1]	352.9	17.964	0.002	15.700	0.001	36.791	0.001
	8N HBr	6 h	[3]	70.7	23.312	0.003	16.229	0.001	37.946	0.001
	7N HNO_3	1 h	[4]	1.5	55.768	0.729	19.365	0.086	39.475	0.072
	15N HNO_3	15 h	[5]	1.2	76.747	1.519	21.425	0.164	40.094	0.112
	48% HF	72 h	[6]	252.5	17.284	0.002	15.625	0.001	35.922	0.001
AW02028	1.5N HBr–2N HCl[a]	5 min	[1]	1102.5	26.353	0.001	16.659	0.001	38.555	0.000
	1N HBr	1 h	[2]	220.0	32.433	0.002	17.247	0.001	39.980	0.001
	8N HBr	6 h	[3]	60.8	67.267	0.022	20.207	0.002	48.089	0.005
	7N HNO_3	1 h	[4]	4.2	43.510	0.169	17.965	0.019	43.039	0.043
	15N HNO_3	15 h	[5]	1.1	64.583	1.234	19.560	0.122	56.343	0.521
	15N HNO_3–48% HF[b]	120 h	[6]	230.0	20.073	0.012	16.048	0.008	37.898	0.002
	48% HF	72 h	[7]	79.5	19.864	0.014	16.017	0.011	38.050	0.003
RD03024	1.5N HBr–2N HCl[a]	5 min	[1]	101.7	16.442	0.002	15.467	0.001	36.162	0.001
	8N HBr	6 h	[3]	54.6	21.164	0.002	15.924	0.001	44.538	0.004
	7N HNO_3	1 h	[4]	0.9	23.688	0.238	16.172	0.050	63.284	0.881
	15N HNO_3	15 h	[5]	1.0	36.854	0.596	17.409	0.079	286.390	7.334
	48% HF	72 h	[7]	53.1	17.990	0.001	15.673	0.001	37.282	0.001

Tourmaline grain size fraction 250–500 μm. Total procedure Pb blanks <20 pg.
[a] Mix = 1.5N HBr and 2N HCl 12:1 mixture.
[b] 1:1 mixture.

et al., 1993) and Arunta Inliers (Raith et al., 2004). Although, tourmaline at Broken Hill is thought to be largely syn-diagenetic or syn-sedimentary (Slack et al., 1993) and in the Arunta tourmaline crystallization is related to the intrusion of leucogranites (Raith et al., 2004).

7.2. Tourmaline U–Th–Pb geochemistry

U–Th–Pb concentrations in the tourmaline were measured by laser ablation ICP-MS (Table 2). The data suggest there is no common template of heavy trace element distribution in these minerals. Tourmaline from Anderson's Lode has relatively high Pb concentrations, but very low U and Th contents. Pb values average 14.0 ppm in cores and 14.9 ppm in rims, U ranges from 0.04 ppm (cores) to 0.02 ppm (rims), while Th shows little variation (mean 0.03 ppm). Average U/Th in this sample is 1.0. Eldorado tourmaline displays decreasing U, Th and Pb abundances from core to rim. Pb ranges from 7.1 ppm in rims to 8.2 ppm in cores, while U decreases from 2.2 ppm in cores to 5.5 ppm in rims. Th varies from 1.5 to 3.6 ppm and average U/Th is 0.6. In contrast, tourmaline from King shows increasing U, Th and Pb concentrations from core to rim. Pb varies from 4.6 ppm in cores to 5.5 ppm in rims, while U ranges from 0.07 to 0.09 ppm and Th averages 0.2–0.3 ppm. The King tourmalines also have the lowest average Th/U ratio (∼0.30) measured in this study.

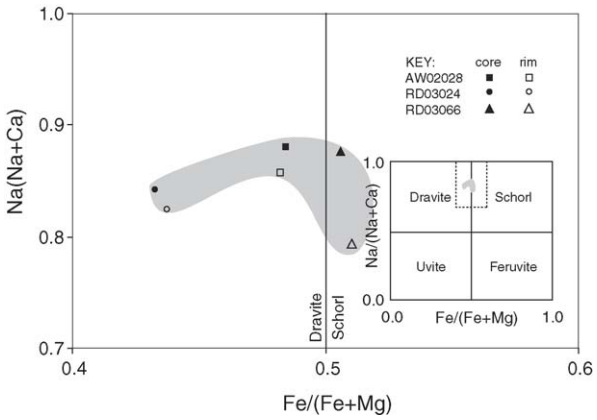

Fig. 7. Plot of Fe/(Fe + Mg) against Na/(Na + Ca) used to classify tourmaline compositions to the schorl-dravite solid solution.

7.3. Scanning electron microprobe imaging of tourmaline

SEM imaging was undertaken to identify possible intra-grain inclusions within the tourmaline that may affect its U–Th–Pb budget, and thus exert some control over the PbSL isotopic patterns. Tourmaline from Anderson's Lode appears to be free from any large inclusions (Fig. 8A). Micron-sized zircons crystallites occur in some grains, but they are spatially restricted to voids on the surfaces of tourmaline crystals (Fig. 8B). Zircons

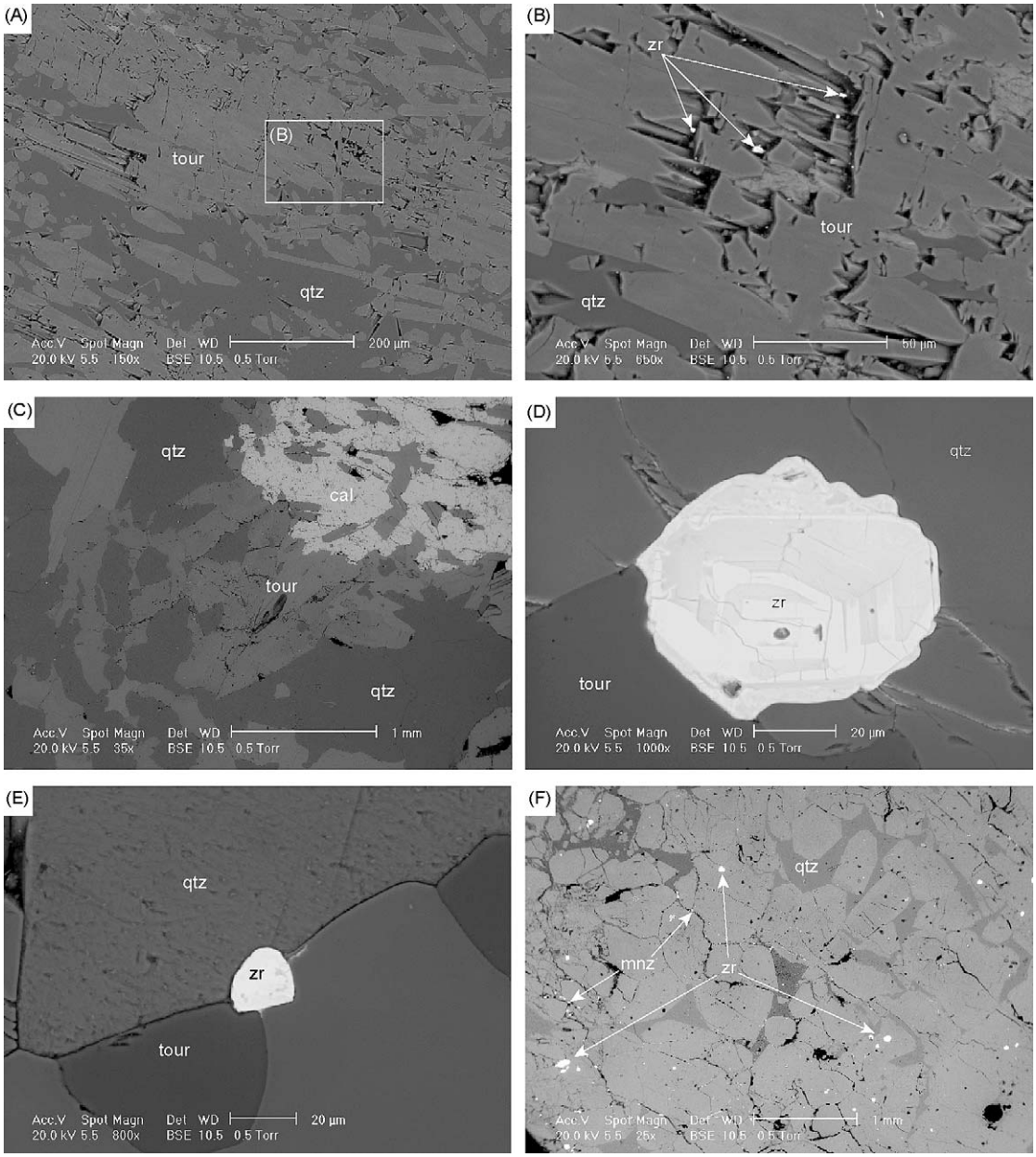

Fig. 8. BSE (back-scattered electron) images of tourmaline samples. (A and B) Sample RD03066 contains few inclusions within the tourmaline (tour) or quartz (qtz), but micron-sized zircon (zr) inclusions do occur on the surface of tourmaline grains. (C–E) Sample AW02028 appears to contain no inclusions, but there are abundant large zircons that are partially enclosed within the tourmaline. (F) Sample RD03024 contains large zircon inclusions hosted in tourmaline grains and later stage monazites (mnz) in veinlets.

of this type should have been removed during sample comminution prior to PbSL. Tourmaline from Eldorado is also free of observable micro-inclusions (Fig. 8C), although abundant zoned and unzoned zircons (10 and 60 μm in diameter) occur in some parts of the tourmaline grains (Fig. 8D and E). These zircons are only partially included within the tourmaline and also should have been removed during sample preparation. Tourmaline from King contains abundant zircons, which are usually completely enclosed by tourmaline crystals, and monazite in veins that cut the tourmaline grains (Fig. 8F).

7.4. Pb stepwise leaching

The Pb isotopic results from the PbSL experiments are given in Table 3. Due to highly variable leach step

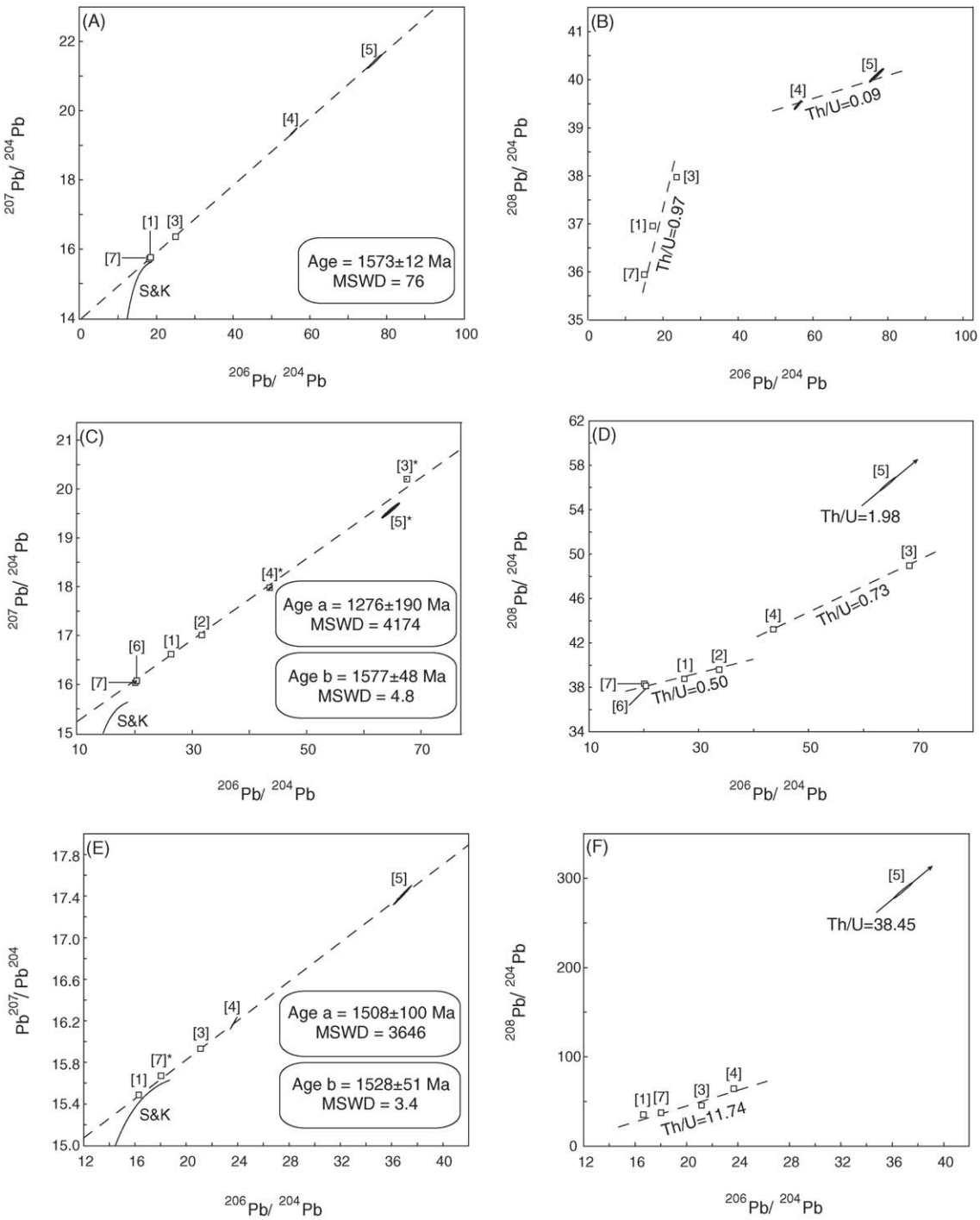

Fig. 9. Pb isotopic plots of PbSL leachates derived form tourmaline separates, constructed using ISOPLOT (Ludwig, 2003); see Table 3 for data. Data points are marked with an asterisk when they are excluded from age calculations. Error ellipses ($\pm 2\sigma_m$) are shown when they exceed the size of the box symbols. Numbers refer to leach step; see Table 3 for details. S&K refers to the Stacey and Kramers (1975) Pb growth curve. (A) ^{207}Pb/^{206}Pb vs. ^{206}Pb/^{204}Pb isochron plot of tourmaline PbSL steps for RD03066. (B) ^{208}Pb/^{206}Pb vs. ^{206}Pb/^{204}Pb (Th/U) discrimination plot of tourmaline PbSL steps for RD03066, also showing zircon and monazite (Th/U) trends. (C) ^{207}Pb/^{206}Pb vs. ^{206}Pb/^{204}Pb isochron plot of tourmaline PbSL steps for AW02028. (D) ^{208}Pb/^{206}Pb vs. ^{206}Pb/^{204}Pb (Th/U) discrimination plot of tourmaline PbSL steps for AW02028, also showing zircon and monazite (Th/U) trends. (E) ^{207}Pb/^{206}Pb vs. ^{206}Pb/^{204}Pb isochron plot of tourmaline PbSL steps for RD03024. (F) ^{208}Pb/^{206}Pb vs. ^{206}Pb/^{204}Pb (Th/U) discrimination plot of tourmaline PbSL steps for RD03024, also showing zircon and monazite (Th/U) trends.

sample sizes (0.5–300 ng Pb), signal sizes on the Nu Plasma MC-ICP-MS varied considerably (0.3–12 V total Pb). Therefore, analytical precisions were also highly variable. Pb isotope data were blank-corrected using a 50 pg blank of Broken Hill galena isotopic composition (Cumming and Richards, 1975); actual blank isotopic compositions scatter around the Broken Hill mean. Errors were propagated using Monte Carlo techniques. Isochron calculations were carried out using ISOPLOT v.3.00 (Ludwig, 2003), with a minimum 2σ input error of 0.03% (in cases where in-run error was <0.03%) to account for uncertainty in the mass bias correction. Blank correction is possible here because Pb quantities in unknowns can be estimated accurately from signal intensities and dilution factors in ICP-MS work. The blank-corrected data invariably produce better isochron fits (lower MSWD) than blank-uncorrected data.

The data in Table 3 show that despite the low overall U/Pb and Th/Pb of the tourmalines, PbSL is able to extract variably radiogenic Pb which can provide meaningful isochron ages (Fig. 9); however, age errors are variable and large in some cases. Radiogenic Pb is extracted mainly in the strong acid steps, which appears to be typical of most silicates (Frei, 1996; Schaller et al., 1997).

Tourmaline from Anderson's Lode (RD03066) yielded five leach steps with a range in $^{206}Pb/^{204}Pb$ of 17.2–76.7 (Fig. 9A). Leach steps 1 and 5 released large amounts of near-common Pb (82% of total Pb released), while the more radiogenic steps (2–4) released very small amounts of Pb; the most uranogenic Pb was released during exposure to 15N HNO_3 in step 4. Thorogenic Pb shows little variation, with $^{208}Pb/^{204}Pb$ ranging from 35.9 to 40.1 (Fig. 9B). Steps 4 and 5 have low calculated Th/U ratios (0.09), indicative of U enrichment in these aliquots. The Th/U ratio of the other steps is around 0.97. Regression of all five leach steps yields a $^{207}Pb/^{206}Pb$ isochron age of 1573 ± 12 Ma (Fig. 9A; MSWD = 76).

The seven leach steps from Eldorado tourmaline (AW02028) yield a wide range in $^{206}Pb/^{204}Pb$ (19.9–67.3). The most uranogenic Pb was released during exposure to 8N HBr; this is uncharacteristic of PbSL on silicates. In contrast with tourmaline from Anderson's Lode, radiogenic Pb is far more abundant in this sample, reflecting the much higher U/Pb ratios (see Table 2), but the release pattern is also visibly non-linear, suggestive of radiogenic components of different ages or variable initial $^{206}Pb/^{207}Pb$. This is reflected by the large MSWD (4174) in a formal isochron regression of all 7 steps (Fig. 9C). The age provided in this regression (1276 ± 190 Ma) is therefore geologically meaningless. Calculated Th/U in steps 3–5 are quite high (0.73 and 1.98) relative to Th/U as measured by laser ablation (0.6). The other steps have lower Th/U close to 0.50. If the high Th/U steps are omitted from the calculation, the resulting four-point age changes to 1577 ± 48 Ma (MSWD = 4.8; Fig. 9C).

PbSL spectra for tourmaline from sample RD03024 (King) yield the narrowest $^{206}Pb/^{204}Pb$ range (16.4–36; Fig. 9E). The highest $^{206}Pb/^{204}Pb$ is released by step 5 and represents only ≈0.5% of the total recovered Pb, it also has an elevated $^{208}Pb/^{204}Pb$ (∼268) signature (Fig. 9F). This suggests the presence of a Th-rich source (perhaps monazite inclusions); however, this step does not appear to be in initial isotopic equilibrium with the other leach steps or it may contain radiogenic components of a different age (see Fig. 9E).

Regression of all leach data for RD03024 produces a five point $^{207}Pb/^{206}Pb$ isochron age of 1508 ± 100 Ma with excessive geological scatter (MSWD = 3646; Fig. 9E). Leach step 7 appears to contribute significantly to the error as it appears to be in isotopic disequilibrium occurring far off the $^{207}Pb/^{206}Pb$ regression line. Age recalculation after the removal of this step yields a four-point $^{207}Pb/^{206}Pb$ isochron age of 1528 ± 51 Ma (MSWD = 3.4). Leach step 7 represents the final dissolution of the samples. Thus, it is most likely step to contain radiogenic components derived from included zircon grains that can only be dissolved in HF (cf. DeWolf et al., 1996), although there is no evidence for this in the $^{208}Pb/^{206}Pb$ values.

8. Discussion

Our results clearly demonstrate the applicability of the PbSL technique to generate Pb–Pb isochrons from tourmaline despite very low and unfavourable bulk U/Pb ratios. The laser ablation data are particularly illustrative in this regard; they demonstrate that the highly variable U/Th and U/Pb ratios encountered during step leaching are not readily resolved in core-rim comparisons. The fact that we observe much higher enrichments in radiogenic Pb confirms the remarkable ability of PbSL to separate common and radiogenic Pb held in separate domains of the host crystal lattice, or in U–Th-rich impurities. The PbSL apparent ages now need to be examined in the context of (poorly known) tourmaline isotopic closure characteristics, estimated metamorphic temperatures, and existing geochronological data.

8.1. Initial isotopic equilibrium or contribution from micro-inclusions?

Although Frei et al. (1997) have shown, for gem-quality titanite, that PbSL isochrons can be generated without significant contributions from U-rich inclusions, the influence of such inclusions needs to be examined on a case-by-case basis. A low MSWD for a PbSL $^{207}Pb/^{206}Pb$ array is a good indicator of a high degree of homogeneity in both common and radiogenic Pb constituents (i.e., a single "age" component) within the target mineral. However, a well-correlated array could simply reflect leakage of uranogenic Pb from U-rich inclusions into several leach steps. In this case, the PbSL array would date the inclusions, not the host mineral. This is of course true for U–Pb dating of low-U minerals in general (e.g. Vance et al., 1998). Obviously, if the impurities are coeval/cogenetic, the resulting PbSL age also dates the host mineral. The ability to trace the Pb in each step via its $^{208}Pb/^{206}Pb$ ratio is useful to determine potential contributions from micro-inclusions (cf. Frei and Kamber, 1995), and this is applied here, in conjunction with the laser ablation data and tourmaline grain imaging.

PbSL for tourmaline from Anderson's Lode produced a well-correlated $^{207}Pb/^{206}Pb$ array for all leach steps (Fig. 9A), confirming the apparent lack of internal inclusions from SEM imaging (Fig. 8A and B). In the $^{208}Pb/^{206}Pb$ (thorogenic) plot two short trends can be defined, with Th/U of 0.09 and 0.97, respectively (Fig. 9B). The Th/U ratios of between 0.81 and 1.39 derived from laser ablation are consistent with the latter steeper trend (Fig. 9B), but do not explain the strong U enrichment in steps 4 and 5, despite the slightly higher U/Th in the cores of Anderson's Lode tourmalines. One possible explanation might involve differential solubility of U- and Th-derived Pb in different parts of the crystal. However, this is rather speculative. The only viable alternative is the presence of low Th/U micro-inclusions, in this case perhaps the zircon crystallites on tourmaline surfaces identified during SEM imaging. As the low-Th/U steps also have the highest $^{206}Pb/^{204}Pb$, the zircons(?) contribute, at least in part, to the isochron.

PbSL data for tourmalines from Eldorado are more heterogeneous than those from Anderson's Lode. In the thorogenic Pb diagram, the leach steps form three distinctive populations. Leach steps 1, 2, 6 and 7 have low calculated Th/U (≈0.50), i.e., much lower than Th/U as determined by laser ablation (1.6–2). Steps 3, 4 and 5 have higher Th/U (0.73 and 1.98; Fig. 9C), that are closer to the Th/U ratios as measured by laser ablation. As is the case with the Anderson's Lode tourmaline, the origin of the low-Th/U components may be linked to the presence of zircon observed in BSE images (Fig. 8D). Thus, it appears that the 1577 ± 48 Ma age for 4 of the 7 PbSL points is based on the very leach steps that have much lower Th/U than is thought to be intrinsic to the tourmaline (i.e., the PbSL age appears to be based on the non-tourmaline components as identified in the thorogenic Pb plot; Fig. 9D).

The tourmaline from King shows relatively homogeneous calculated Th/U (∼12) in 4 of 5 leach steps (Fig. 9F). Step 5 is clearly different, with an elevated inferred Th/U ∼38. Such a high ratio is in excess of that measured by laser ablation (<4), and far higher than in most minerals or bulk crust. Strongly thorogenic Pb could be derived from monazite inclusions (e.g., DeWolf et al., 1996), although Th/U > 10 would be unusual for monazite. SEM images of these tourmalines show monazite in late stage veins in King tourmaline, but it is not evident in the tourmaline itself from either BSE imaging or from irregular laser ablation data. This would also tend to rule out the presence of sub-micron Th-rich inclusions. Furthermore, the numerous zircon crystals identified in King tourmalines would be an unlikely source for such extremely thorogenic Pb. Unless we appeal to other, unidentified inclusions, or to some process that fractionates thorogenic from uranogenic Pb during the leaching processes, no explanation can be offered for the highly unusual ^{208}Pb-rich nature of the King tourmaline PbSL steps at this stage.

Overall, inclusion-derived radiogenic Pb appears to be present in all three tourmaline samples, and it is therefore likely that the observed PbSL isotopic arrays are generated by Pb released from both the tourmaline lattice and from inclusions. The apparent ages from 1.58 to 1.53 Ga are within the range of the Isan Orogeny and thus appear geologically reasonable given the relative timing constraints of the tourmalines. Presumably, this implies that the U-rich inclusions in the tourmalines are cogenetic or at least of similar age.

8.2. Pb closure temperature in tourmaline: age implications

Given the paucity of geochronological studies involving tourmaline, there is little published information on tourmaline closure temperatures. Andriessen et al. (1991) suggested that Ar closure temperatures (T_c) may be higher in tourmaline than in hornblende (i.e., greater than 500 °C depending on cooling rate, mineral grain size, etc.). However, we are not aware of any empirical or experimental T_c data for Pb in tourmaline. A method

to estimate isotope closure temperature based on the concept of ionic porosity was applied to the U–Pb system by Dahl (1997).

The ionic porosity, Z, is defined as the percentage of the mineral unit cell volume unoccupied by ions (Dowty, 1980; Fortier and Giletti, 1989). For application to U–Pb isotope data, Dahl (1997) extrapolated two linear T_c-Z calibrations for Pb retentivity:

$$T_c \text{ low (Pb)} \approx -34.7 \times Z + 1809 \quad (1)$$

$$T_c \text{ high (Pb)} \approx -45.0 \times Z + 2201. \quad (2)$$

Based on unit cell data from Deer et al. (1992), ionic radii from Shannon and Prewitt (1969) and electron microprobe data for each tourmaline sample (Table 1), Z has been calculated as ≈35% for all three dated samples, resulting in estimated closure temperatures that range from ≈580 to 630 °C (schorlitic compositions lower the T_c).

At Anderson's Lode, tourmaline veins formed prior to the metamorphic peak, represented by a mid-greenschist facies biotite-chlorite assemblage. Temperatures are unlikely to have exceeded likely closure temperatures; the 1573 Ma PbSL tourmaline age thus reflects the age of tourmaline formation. At Eldorado and King, peak-metamorphic temperatures reached 540–640 and ≈600 °C, respectively (Connors, 1992; Rubenach, 1992). At these locations the metamorphic temperatures are similar to estimated tourmaline closure temperatures, and thus the ages may potentially reflect cooling.

It should be noted, however, that closure temperatures for tourmaline alone, even if the estimates above are accurate, are unlikely to be the only determining factor for isotopic equilibration. Firstly, if zircon and other accessory minerals contributed to the PbSL ages, the closure behaviour of these phases will also play a role. Secondly, apparent post-formation (cooling) mineral ages may reflect processes other than just volume diffusion (an assumption made in the closure temperature concept). Other factors, such as passage of deformation and recrystallization fronts through the mineral, or further growth of the same mineral during a discrete younger event, are likely to affect mineral ages (Villa, 1998). Nevertheless, the PbSL ages obtained here appear to be geologically reasonable, and their possible significance will be discussed below.

8.3. Implications for the timing of metamorphism and tectonism

The relative timing criteria imply that tourmalinization at Anderson's Lode and Eldorado are syn-D_2 in timing. Therefore, we can assign an age of ~1575 Ma to this event. This is consistent with the 1575 Ma U–Pb age for peak-metamorphic monazite from the ECV (Hand and Rubatto, 2002), and is similar to ~1565 Ma $^{207}Pb/^{206}Pb$ ages for zircons from pegmatites south of Mount Isa (Connors and Page, 1995). However, the same authors favour an age ~1530 Ma for the D_2 event. In contrast, Perkins et al. (1999) report Ar–Ar ages of 1554–1534 Ma that represent cooling after peak metamorphism in the ECV near Anderson's Lode.

Structural relationships at King demonstrate that tourmaline formation is post-D_2, but pre-D_{3a} and thus probably younger than 1530 Ma (cf. 1510 Ma age for D_3 deformation in the Sybella Batholith; Page and Bell, 1986). This is consistent with the (imprecise) PbSL age of 1528 ± 51 Ma for King tourmaline.

We interpret the early ages of ~1575 Ma to provide a chronological constraint for the onset of metamorphism in the Western Fold Belt. Younger Ar–Ar dates for metamorphic biotite at Anderson's Lode (Perkins et al., 1999) reflect the much lower closure temperature of Ar diffusion in biotite compared with that of U/Pb in tourmaline. It is important to note that the spread of dates from 1575 to 1530 Ma present an opportunity to study the length of elevated heat flow associated with the regional HT-LP metamorphism in the WFB. This window reflects the prolonged duration of tectonic shortening during the Isan Orogeny. It appears that regional tourmalinization and silicification resulted from at least two discrete hydrothermal episodes over at least 45 myr during the same orogenic event. The later thermal episode, involving tourmaline formation at ~1530 Ma, corresponds in time with the peak of magmatic activity during the Williams thermal event in the EFB (Fig. 3; Oliver et al., 2004; and references therein).

The duration of the Isan Orogeny in the WFB as defined here fits into the 1590–1500 Ma timescale for the entire Mount Isa Inlier, as provided by relative chronological evidence in O'Dea et al. (1997). The new ~1575 Ma age for metamorphism, D_2 deformation and associated metamorphic fluid flow in the WFB favoured here is similar to estimates of 1585–1570 Ma for peak metamorphism in the EFB (e.g., Page and Sun, 1998; Perkins and Wyborn, 1998; Giles and Nutman, 2002). If correct, this apparent correlation would suggest that metamorphism was broadly synchronous across the entire inlier, this differs from previous tectonic interpretations for the inlier (e.g., MacCready et al., 1998; Giles and Nutman, 2002) and has fundamental implications for geodynamic modelling of the Isan Orogeny. For example, it would imply that structural styles cannot be used categorically to identify deformational

timing relationships over large areas (e.g., Connors, 1992).

8.4. Implications for fluid flow, partial melting and mineralization

Compositions of the least radiogenic Pb in the tourmaline PbSL arrays plot near the Pb growth curve in $^{207}Pb/^{206}Pb$ space (Fig. 9). This suggests an evolved upper crustal source (Stacey and Kramers, 1975; Zartman and Doe, 1981; Tilton, 1983) for the common Pb incorporated in the tourmalines during crystallization and that the Pb source is significantly older than metamorphism and tourmaline formation. This excludes a mantle-derived magmatic fluid source. This is consistent with initial tourmaline Pb compositions that close mirror ECV Pb isotope data (Gulson et al., 1983; Carr et al., 2004).

Boron contents of mafic volcanics, such as the ECV which host the studied tourmalines at Anderson's Lode and Eldorado, are typically too low to promote the formation of borosilicate minerals (e.g., Henry and Dutrow, 1996). External boron sources, such as metasedimentary units present within and overlying the ECV, must have contributed to the B budget of the system. A possible mechanism involves the mobilization of B from metasedimentary rocks as a result of the metamorphic decomposition of mica and chlorite. Mobile B was then transported into suitable chemical traps within the ECV by metamorphic fluids and/or melts. Conceivably, this would also facilitate mixing of mobile Pb from the metasediments and ECV, possibly explaining some of the scatter in the PbSL isochrons.

In the areas that underwent relatively higher grades of metamorphism (i.e., west of the Mount Isa fault) tourmaline-bearing lithologies are far more abundant and net boron metasomatism can be demonstrated on ~100 m scales from the actual tourmaline-bearing pegmatite or tourmalinites. This implies that the tourmaline may have been the result of fluid-driven crustal partial melting; in which boron was concentrated prior to its release was a hydrothermal fluid (with no discernible mantle magmatic signature). Thus, the tourmaline dates reflect thermal peaks within the Isan Orogeny in the WFB.

8.5. Potential implications for mineralization

The spatial relationship of tourmaline with small Cu and U deposits, along with the paragenetic association with minor sulphide and oxide phases suggest that during hydrothermal fluid movement driven by metamorphism, metals of economic interest were mobile.

Leach spectra from the Anderson's Lode tourmaline sample show U enrichment synchronous with tourmaline crystallization and the Eldorado sample contains primary fluid inclusions with elevated U (Duncan and Wilde, 2004) suggesting a link between tourmaline alteration and U-rich fluid flow. Due to the geochemical mobility of U it is not known if this represents remobilization during the early stages of metamorphism or primary mineralization. U mineralization around Mount Isa has been found to be pre- to early syn-metamorphic in timing (Gregory et al., 2005), supporting either interpretation. The syn-metamorphic remobilization of U formed the relatively large Mary Kathleen U-REE deposit in the EFB (Page, 1983; Maas et al., 1987; Oliver et al., 1999).

The regional association of tourmaline with large volumes of silicification may indicate that the silica-rich halo around the Cu ore bodies formed at a similar time (i.e. ca. 1575 Ma). Relative timing criteria in the Mount Isa Cu ore bodies suggest that silicification was the result of a pre-copper fluid flow event that was contemporaneous with the Isan Orogeny (Wilde et al., 2005). It is widely thought that the ECV are the source of Cu for Mount Isa deposits (e.g., Heinrich et al., 1995; Hannan et al., 1993; Gregory, 2005). The fluid(s) generated by the partial melting event mentioned above may have mobilized large amounts of Cu, as well as generating the tourmaline occurrences.

9. Summary

This study represents one of the first applications of PbSL dating to tourmalines. Although complications due to U- or Th-rich micro-inclusions exist, the results clearly indicate the ability of PbSL to extract meaningful Pb–Pb ages from low-U tourmalines. The PbSL ages obtained here (1575–1530 Ma) are consistent with relative timing criteria based on paragenesis and microstructures, and with other age data for the Isan Orogeny in the WFB around Mount Isa. A model closure temperature of ≈600 °C for tourmaline has been calculated based on the ionic porosity model for Pb retentivity. Comparison of independent estimates of peak-metamorphic temperatures suggests the PbSL ages represent mineral formation, rather than cooling ages. At least two episodes of metamorphic/hydrothermal tourmaline formation in the ECV and Myally Subgroup relate to thermal events in both the WFB and EFB. Similar ~1575 Ma ages for metamorphism in the WFB and EFB are incompatible with current geodynamic models that suggest a bipartite tectonic evolution for the Mount Isa Inlier from 1600 Ma.

Acknowledgements

The Pb step-leaching routine presented here are derived from the unpublished intellectual property of J. Hergt, J. Woodhead and M. Tonelli (University of Melbourne). Without their effort this work would not have been possible. Work reported here forms part of RJD's PhD within the pmd*CRC (Predictive Minerals Discovery Cooperative Research Centre) with support from Xstrata Copper, and this paper is published with permission. Many thanks to N. Oliver and K. Eriksson for reviewing this manuscript and providing invaluable comments.

References

Andriessen, P.A.M., Hebeda, E.H., Simon, O.J., Verschure, R.H., 1991. Tourmaline K–Ar ages compared to other radiometric dating systems in Alpine anatectic leucosomes and metamorphic rocks (Cyclades and Southern Spain). Chem. Geol. 91, 33–48.

Bell, T.H., 1983. Thrusting and duplex formation at Mount Isa, Queensland, Australia. Nature 304, 493–497.

Betts, P.G., Lister, G.S., O'Dea, M.G., 1998. Asymmetric extension of the middle Proterozoic lithosphere, Mount Isa terrane, Queensland, Australia. Tectonophysics 296, 296–316.

Buick, I.S., Frei, R., Cartwright, I., 1999. The timing of high-temperature retrogression in the Reynolds Range, central Australia: constraints from garnet and epidote Pb–Pb dating. Contrib. Mineral. Petr. 135, 244–254.

Carr, G.R., Denton, G.J., Parr, J., Sun, S., Korsh, M.J., Bodon, S.B., 2004. Lightning does strike twice: multiple ore events in major mineralized systems in northern Australia. In: Muhling, J., et al. (Eds.), SEG 2004: Predictive Mineral Discovery Under Cover; Extended Abstracts. University of Western Australia, pp. 332–335.

Collerson, K.D., Kamber, B.S., Schoenberg, R., 2002. Applications of accurate, high-precision Pb isotope ratio measurement by multi-collector ICP-MS. Chem. Geol. 188, 65–83.

Connors, K.A., 1992. Tectonothermal Evolution of the Mount Novit Ranges, Mount Isa Inlier, Australia. Monash University, 242 pp (unpubl.).

Connors, K.A., Lister, G.S., 1995. Polyphase deformation in the western Mount Isa Inlier, Australia: episodic or continuous deformation? J. Struc. Geol. 17, 305–328.

Connors, K.A., Proffett, J.M., Lister, G.S., Scott, R.J., Oliver, N.H.S., Young, D.J., 1992. Geology of the Mount Novit Ranges, southwest of Mount Isa mine. In: Stewart, A.J., Blake, D.H. (Eds.), Detailed studies of the Mount Isa, Inlier, Aust., Geol., Surv., Organ, Bull., vol. 243, pp. 137–160.

Connors, K.A., Page, R.W., 1995. Relationships between magmatism, metamorphism and deformation in the western Mount Isa Inlier, Australia. Precambrian Res. 71, 131–153.

Cumming, G.L., Richards, J.R., 1975. Ore lead isotope ratios in a continuously changing earth. Earth Planet. Sci. Lett. 28, 155–171.

Dahl, P.S., 1997. A crystal-chemical basis for Pb retention and fission-track annealing systematics in U-bearing minerals, with implication for geochronology. Earth Planet. Sci. Lett. 150, 277–290.

Dahl, P.S., Foland, K.A., Holm, D.K., Gardner, E.T., Hubacher, F.A., 1999. New constraints on the timing of Early Proterozoic tectonism in the Black Hills (South Dakota), with implications for docking of the Wyoming province with Laurentia. Bull. Geol. Soc. Am. America 111, 1335–1349.

Dahl, P.S., Frei, R., 1998. Step-leach Pb–Pb dating of inclusion-bearing garnet and staurolite, with implications for early Proterozoic tectonism in the Black Hills collisional orogen, South Dakota, United States. Geology 26, 111–114.

Deer, W.A., Howie, R.A., Zussman, J., 1992. An Introduction to the Rock Forming Minerals. Wiley, New York.

DeWolf, C.P., Zeissler, C.J., Halliday, A.N., Mezger, K., Essene, E.J., 1996. The role of inclusions in U–Pb and Sm–Nd garnet geochronology: step-wise dissolution experiments and trace uranium mapping by fission track analysis. Geochim. Cosmochim. Acta 60, 121–134.

Dowty, E., 1980. Crystal-chemical factors affecting the mobility of ions in minerals. Am. Mineral. 65, 174–182.

Duncan, R.J., Wilde, A.R., 2004. Tourmaline at Mount Isa, Australia: a tracer of metal-rich hydrothermal fluid flow. In: Mulhing, J., et al. (Eds.), SEG 2004 Predictive Mineral Discovery Under Cover; Extended Abstracts. University of Western Australia, p. 413.

Eriksson, K.A., Simpson, E.L., Jackson, M.J., 1994. Stratigraphical evolution of a Proterozoic syn-rift to post-rift basin: constraints on the nature of lithospheric extension in the Mount Isa Inlier, Australia. In: Frostick, L.E. (Ed.), Tectonic controls and signatures in sedimentary successions. Blackwell Scientific, pp. 203–221.

Fortier, S.M., Giletti, B.J., 1989. An empirical model for predicting diffusion coefficients in silicate minerals. Science 245 (4925), 1481–1484.

Frei, R., 1996. The extent of inter-mineral isotope equilibrium: a systematic bulk U–Pb and Pb step leaching (PbSL) isotope study of individual minerals from the Tertiary granite of Jerissos (northern Greece). Eur. J. Mineral. 8, 1175–1189.

Frei, R., Biino, G.G., Prospert, C., 1995. Dating a Variscan pressure-temperature loop with staurolite. Geology 23, 1095–1098.

Frei, R., Kamber, B.S., 1995. Single mineral Pb–Pb dating. Earth Planet. Sci. Lett. 129, 261–268.

Frei, R., Kramers, J.D., Nagler, T.F., Schonberg, R., 1998. Re–Os, Sm–Nd, U–Pb, and stepwise lead leaching isotope systematics in shear-zone hosted gold mineralization: genetic tracing and age constraints of crustal hydrothermal activity. Geochim. Cosmochim. Acta 62, 1925–1936.

Frei, R., Kramers, J.D., Przybylowicz, W.J., Prozesky, V.M., Hofmann, B.A., Kamber, B.S., Villa, I.M., Nagler, T.F., 1997. Single mineral dating by the Pb–Pb step-leaching method: assessing the mechanisms. Geochim. Cosmochim. Acta 61, 393–414.

Frei, R., Pettke, T., 1996. Mono-sample Pb–Pb dating of pyrrhotite and tourmaline: Proterozoic vs. Archean intracratonic gold mineralization in Zimbabwe. Geology 24, 823–826.

Gale, N.H., 1996. A new method for extracting and purifying lead from difficult matrices for isotopic analysis. Anal. Chim. Acta 332, 15–21.

Giles, D., Nutman, A.P., 2002. SHRIMP U–Pb monazite dating of 1600-1580 Ma amphibolite facies metamorphism in the southeastern Mt Isa Block, Australia. Aus. J. Earth Sci. 49, 455–465.

Gregory, M.J., 2005. The Geological Evolution of the Eastern Creek Volcanics, Mount Isa, Australia and Implications for the Mount Isa Copper Deposit. Monash University, 165 pp (unpubl.).

Gregory, M.J., Wilde, A.R., Jones, P.A., 2005. Uranium deposits of the Mount Isa Region and their relationship to deformation, metamorphism and copper deposition. Econ. Geol. 100, 537–546.

Gulson, B.L., Perkins, W.G., Mizon, K.J., 1983. Lead isotope studies bearing on the genesis of the copper ore bodies at Mount Isa, Queensland. Econ. Geol. 78, 1466–1504.

Hand, M., Rubatto, D., 2002. The scale of the thermal problem in the Mt. Isa Inlier. In: Preiss, V.P. (Ed.), Geoscience 2002: Expanding Horizons. Abstracts of the 16th Australian Geological Convention, Adelaide, pp. 173.

Hannan, K.W., Golding, S.D., Herbert, H.K., Krouse, H.R., 1993. Contrasting alteration assemblages in metabasites from Mount Isa, Queensland; implications for copper ore genesis. Econ. Geol. 88, 1135–1175.

Hawthorne, F.C., Henry, D.J., 1999. Classification of the minerals of the tourmaline group. Eur. J. Mineral. 11, 201–215.

Heinrich, C.A., Bain, J.H.C., Mernagh, T.P., Wyborn, L.A.I., Andrew, A.S., Waring, C.L., 1995. Fluid and mass transfer during metabasalt alteration and copper mineralization at Mount Isa, Australia. Econ. Geol. 90, 705–730.

Henry, D.J., Dutrow, B.L., 1996. Metamorphic tourmaline and its petrological implications. In: Grew, E.S., Anovitz, L.N. (Eds.), Boron: Mineralogy, Petrology and Geochemistry. Rev. Mineral., vol. 33, pp. 503–557.

Henry, D.J., Guidotti, C.V., 1985. Tourmaline as a petrogenetic indicator mineral: an example from the staurolite-grade metapelites of NW Maine. Am. Mineral. 70, 1–15.

Kamber, B.S., Frei, R., Gibb, A.J., 1998. Pitfalls and new approaches in granulite chronometry. An example from the Limpopo Belt, Zimbabwe. Precambrian Res. 91, 69–285.

Lanzirotti, A., Hanson, G.N., 1997. An assessment of the utility of staurolite in U–Pb dating of metamorphism. Contrib. Mineral. Petr. 129, 352–365.

Ludwig, K., 2003. Users Manual for Isoplot 3.00: A geochronological toolkit for Microsoft Excel. Berkeley Geochronological Centre Special Publication 4, Berkeley, California, pp. 70.

Maas, R., McCulloch, M.T., Campbell, I.H., 1987. Sm–Nd isotope systematics in uranium-rare earth element mineralization at the Mary Kathleen uranium mine, Queensland. Econ. Geol. 82, 1805–1826.

MacCready, T., Lister, G.S., Goleby, B.R., Goncharov, A., Drummond, B.J., 1998. A framework of overprinting orogens based on interpretation of the Mount Isa deep seismic transect. Econ. Geol. 93 (8), 1422–1434.

Mathias, B.V., Clark, G.J., 1975. Mount Isa copper and silver–lead–zinc ore bodies: Mount Isa and Hilton Mines. In: Knight, C.L. (Ed.), Economic Geology of Australia and Papua New Guinea: I Metals. Aust. Inst. Min. Metall., Monograph 5, pp. 351–372.

Mezger, K., Rawnsley, C.M., Bohlen, S.R., Hanson, G.N., 1991. U–Pb garnet, sphene, monazite, and rutile ages: implications for the duration of high-grade metamorphism and cooling histories, Adirondack Mts., New York. J. Geol. 99, 415–428.

Müller, W., 2003. Strengthening the link between geochronology, textures and petrology. Earth Planet. Sci. Lett. 206, 42–47.

O'Dea, M.G., Lister, G., MacCready, T., Betts, P.G., Oliver, N.H.S., Pound, K.S., Huang, W., Valenta, R.K., 1997. Geodynamic evolution of the Proterozoic Mount Isa Terrain. In: Burg, J.-P., Ford, M. (Eds.), Orogeny Through Time. Geological Society of London Special Publication, vol. 121, pp. 99–122.

Oliver, N.H.S., Pearson, P.J., Holcombe, R.J., Ord, A., 1999. Mary Kathleen metamorphic-hydrothermal uranium-rare-earth element deposit: ore genesis and numerical model of coupled deformation and fluid flow. Aus. J. Earth Sci. 46, 467–484.

Oliver, N.H.S., Cleverley, J.S., Mark, G., Pollard, P.J., Fu, B., Marshall, L.J., Rubenach, M.J., Williams, P.J., Baker, T., 2004. Modelling of the role of sodic alteration in the genesis of iron-oxide-copper-gold deposits, Eastern Mount Isa Block, Australia. Econ. Geol. 99, 1145–1176.

Page, R.W., 1983. Chronology of magmatism, skarn formation and uranium mineralization, Mary Kathleen, Queensland, Australia. Econ. Geol. 78, 838–853.

Page, R.W., Bell, T.H., 1986. Isotopic and structural responses of granite to successive deformation and metamorphism. J. Geol. 94, 365–379.

Page, R.W., Sun, S.-S., 1998. Aspects of geochronology and crustal evolution in the Eastern Fold Belt, Mt Isa Inlier. Aus. J. Earth Sci. 45, 343–361.

Pearce, N.J.G., Perkins, W.T., Westgate, J.A., Gorton, M.P., Jackson, S.E., Neal, C.R., Chenery, S.P., 1997. A compilation of new and published major and trace element data for NIST SRM 610 and NIST SRM 612 glass reference materials. Geostandard. Newslett. 21, 115–144.

Perkins, C., Heinrich, C.A., Wyborn, L.A.I., 1999. $^{40}Ar/^{39}Ar$ geochronology of copper mineralization and regional alteration, Mount Isa, Australia. Econ. Geol. 94, 23–36.

Perkins, C., Wyborn, L.A.I., 1998. Age of Cu–Au mineralization, Cloncurry district, eastern Mt Isa Inlier, Queensland, as determined by $^{40}Ar/^{39}Ar$ dating. Aus. J. Earth Sci. 45, 33–246.

Raith, J.G., Riemer, N., Schöner, N., Meisel, T., 2004. Boron metasomatism and behaviour of rare earth elements during formation of tourmaline rocks in the eastern Arunta Inlier, central Australia. Contrib. Mineral. Petr. 147, 91–109.

Roberts, M.P., Finger, F., 1997. Do U–Pb zircon ages from granulites reflect peak metamorphic conditions? Geology 25, 319–322.

Rubenach, M.J., 1992. Proterozoic low-pressure/high-temperature metamorphism and an anticlockwise P-T-t path for the Hazeldene area, Mount Isa Inlier, Queensland, Australia. J. Metamorph. Geol. 10, 333–346.

Schaller, M., Kramers, J.D., Steiner, O., Studer, I., Frei, R., 1997. Pb stepwise leaching (PbSL) dating of garnet—addressing the inclusion problem. Schweiz. Miner. Petrog. 77, 113–121.

Shannon, R.D., Prewitt, C.T., 1969. Effective ionic radii in oxides and flourides. Acta Crystallogr. B25, 925–946.

Slack, J.F., 1982. Tourmaline in Appalachian—Caledonian massive sulphide deposits and its exploration significance. T.I. Min. Metall. B 91, 81–89.

Slack, J.F., Palmer, M.R., Stevens, B.P.J., Barnes, R.G., 1993. Origin and significance of tourmaline-rich rocks in the Broken Hill district, Australia. Econ. Geol. 88, 505–541.

Spikings, R.A., Lister, G.S., Foster, D.A., Kohn, B.P., 2002. Post-orogenic (<1500 Ma) thermal history of the Palaeo-Mesoproterozoic Eastern Fold Belt, Mount Isa Inlier, NE Australia. Tectonophysics 109, 103–144.

Stacey, J.S., Kramers, J.D., 1975. Approximation of terrestrial Pb isotope evolution by a two-stage model. Earth Planet. Sci. Lett. 26, 207–221.

Thériault, R.J., Davies, W.J., 1999. Rapid extraction of Sr and Pb from ion-specific chromatography for thermal ionisation mass spectrometry analysis. Radiogenic Age Isotopic Stud. Rep. 12, 9–12.

Tilton, G.R., 1983. Evolution of depleted mantle: the lead perspective. Geochim. Cosmochim. Acta 47, 1191–1197.

van Achterbergh, E., Ryan, C., Jackson, S., Griffin, W., 2001. Data reduction software for LA-ICP-MS. In: Sylvester, P. (Ed.), Laser Ablation-ICPMS in the Earth Sciences. Mineral Assoc. Can. Short Course Handbook, vol. 29, pp. 239–243.

Vance, D., Meier, M., Oberli, F., 1998. The influence of high U–Th inclusions on the U–Th–Pb systematics of almandine-pyrope garnet: results of a combined bulk dissolution, stepwise-leaching, and SEM study. Geochim. Cosmochim. Acta. 62, 3527–3540.

Villa, I.M., 1998. Isotopic closure. Terra Nova 10, 42–47.

Wilde, A.R., Gregory, M.J., Duncan, R.J., Gessner, K., Kühn, M., Jones, P., 2005. Geochemical process model for the Mt Isa Cu–Co–Ag deposits. In: Mao, J., Bierlein, F.P. (Eds.), Eighth Biennial SGA Meeting—Mineral Deposit Research: Meeting the Global Challenge, Beijing, pp. 199–202.

Williams, M.L., Jercinovic, M.J., 2002. Microprobe monazite geochronology: putting absolute time into microstructural analysis. J. Struc. Geol. 24, 1013–1028.

Woodhead, J.D., 2002. A simple method for obtaining highly accurate Pb isotope data by MC-ICP-MS. J. Anal. Atom. Spec. 17, 1–6.

Wyborn, L.A.I., Page, R.W., McCulloch, M.T., 1998. Petrology, geochronology and isotope geochemistry of the post-1820 Ma granites of the Mount Isa Inlier: mechanisms for the generation of Proterozoic anorogenic granites. Precambrian Res. 40/41, 509–541.

Zartman, R.E., Doe, B.R., 1981. Plumbotectonics—the model. Tectonophysics 75, 135–162.